



## Orientation mediated self-assembled gallium phosphide islands grown on silicon

V. NARAYANAN<sup>†</sup>, S. MAHAJAN

Department of Chemical, Bio and Materials Engineering,  
and Center for Solid State Electronic Research,  
Arizona State University, Tempe, AZ 85287-6006, USA

N. SUKIDI<sup>‡</sup>, K. J. BACHMANN<sup>‡</sup>, V. WOODS<sup>§</sup> and N. DIETZ<sup>§</sup>

<sup>‡</sup> Department of Materials Science and Engineering and  
<sup>§</sup> Department of Physics, North Carolina State University,  
Raleigh, NC 27695-7919, USA

[Received 7 December 1998 and revised version accepted 22 April 1999]

### ABSTRACT

Evolution of gallium phosphide epitaxial islands, grown on the (001), (111), (110) and (113) surfaces of Si by chemical beam epitaxy, has been investigated by p-polarized reflectance spectroscopy, transmission electron microscopy and atomic force microscopy. The growth nucleates as faceted three-dimensional islands on the (001) and (111) Si surfaces because of the polar nature of the heterointerface which increases the interfacial energy. A more two-dimensional-like growth mode is seen on the (110) and (113) surfaces which is attributed to the absence of charge build up at the GaP–Si heterointerface for these orientations, thereby reducing the interface energy. Islands grown on (001) Si become more faceted and larger in size with increase in growth temperature. This is due to a lower incubation time and enhanced atomic mobility at high temperatures. Wurtzite GaP has been observed to coexist with the zincblende polytype in some of the islands grown on (111) Si at 560°C. Arguments have been developed to rationalize these observations.

### §1. INTRODUCTION

GaP and Si exhibit a lattice mismatch of 0.37% at room temperature. Therefore, the two materials constitute a nearly ideal combination for the integration of Si and III–V technologies. A number of previous studies have indicated that GaP nucleates on (001) Si in the form of islands (Ernst and Pirouz 1988, 1989, Soga *et al.* 1991, 1994, 1996). These islands exhibit a high density of planar defects despite the low lattice mismatch (Ernst and Pirouz 1988, 1989). Further, the island shape and planar defect morphology are remarkably similar to those observed in GaAs–Si (001), a system with a large lattice mismatch of 4% (Gerthsen *et al.* 1990, Vila *et al.* 1993, 1997). This suggests that planar defect formation in GaP–Si may not arise from misfit stresses, but rather from growth mistakes on faceted GaP islands. If indeed this is the case, then it is important to understand the evolution of these facets.

---

<sup>†</sup> E-mail: vijayn@asu.edu

However, this issue has not been examined in detail as a function of growth parameters, although a few studies, for example Vila *et al.* (1997), have reported on the morphology of epitaxial GaAs islands grown on (001) Si. They have observed that islands were either faceted on {111} or {113} planes. Islands terminated by {111} facets exhibit planar defects parallel to the facet plane, while those terminated by {113} facets show misfit dislocations at the layer-substrate interface.

In the present study, we have investigated the initial stages of heteroepitaxy of GaP on the low index (001) and (111) Si, the two most widely used substrate orientations in microelectronics. However, the GaP-Si heterointerface for both these orientations is not charge neutral. The corresponding charge build up would increase the interfacial energy. To delineate the effect of interface charge on growth morphology, we have extended this work to the (110) and (113) surfaces since the heterointerface between GaP and Si for these two interfaces would be electrically neutral (Kroemer *et al.* 1980, Chadi 1984). Growth on vicinal GaAs-Si (110) tilted towards [001] has revealed planar defect free films with the better film morphology being attributed to step flow growth mode (Yodo *et al.* 1994). However, the initial stages of growth were not investigated and the explanation was proposed on the basis of the quality of thick films. The (113) Si surface has been receiving a lot of attention in recent years because of its high stability similar to that of the low index planes (Knall and Pethica 1992, Hadley *et al.* 1993). Although the (113) surface could provide superior interface properties during growth, our growths are the first documented attempts on heteroepitaxy of III-V on Si (113).

The present paper reports on the results of transmission electron microscopy (TEM), atomic force microscopy (AFM) and p-polarized reflectance spectroscopy (PRS) studies obtained from the initial stages of epitaxial growth of GaP on the (001), (111), (110) and (113) surfaces of silicon by chemical beam epitaxy (CBE). Our emphasis here is to discern the effects of orientation on the nucleation and morphology of GaP islands.

## §2. EXPERIMENTAL PROCEDURE

The Si wafers were cleaned using a procedure consisting of a ten minute dip in a 1:1:5 solution of  $\text{NH}_4\text{OH}$ ,  $\text{H}_2\text{O}_2$  and deionized (DI) water maintained at  $75^\circ\text{C}$ , a five minute rinse in DI water, a ten minute dip in a 1:1:5 solution of  $\text{HCl}$ ,  $\text{H}_2\text{O}_2$  and DI water also kept at  $75^\circ\text{C}$  and a rinse in DI water. This was followed by a buffered HF etch and a final DI water rinse.

The substantial difference in the coefficient of thermal expansion between GaP and Si warrants low temperature growth processing to minimize the thermal strains generated during cooling after growth. Therefore, we have used CBE. GaP was deposited on exactly oriented Si substrates under the conditions of pulsed chemical beam epitaxy (Kelliher *et al.* 1993). The heated Si substrate was exposed to pulses of tertiarybutylphosphine (TBP) and triethylgallium (TEG) with a steady hydrogen background pressure. The duration of the source vapour cycle  $t_{\text{src}}$  repeated throughout the growth run was made up of the widths of the TBP and TEG pulses and pauses in between. For  $t_{\text{src}}$  on the order of a few seconds, the length of the pause after the TBP pulses did not significantly affect the growth rate, but the length of the pause after the TEG pulses did, i.e. the provision of a period of time after each pulse for migration-enhanced growth was ineffective for TBP, but was effective for TEG (Bachmann *et al.* 1995b). Thus, in these experiments, the substrate was exposed to

pulses of TEG while TBP was maintained at a steady flow in order to increase the phosphorus supersaturation.

The fluxes of the precursors and hydrogen were controlled by mass flow controllers, and the timing of the precursors' injection into the reactor was achieved by a microprocessor which was also used synchronously for data acquisition with 10 Hz resolution. The temperature range investigated was 350–560°C and the overall pressure during deposition was between  $10^{-4}$  and  $10^{-5}$  Torr. Using a cycle time  $t_{\text{svc}}$  of 5 s, TEG flow of 0.05 sccm was pulsed into the reactor for 300 ms per cycle under continuous TBP and hydrogen flow of 0.6 sccm and 5.0 sccm respectively.

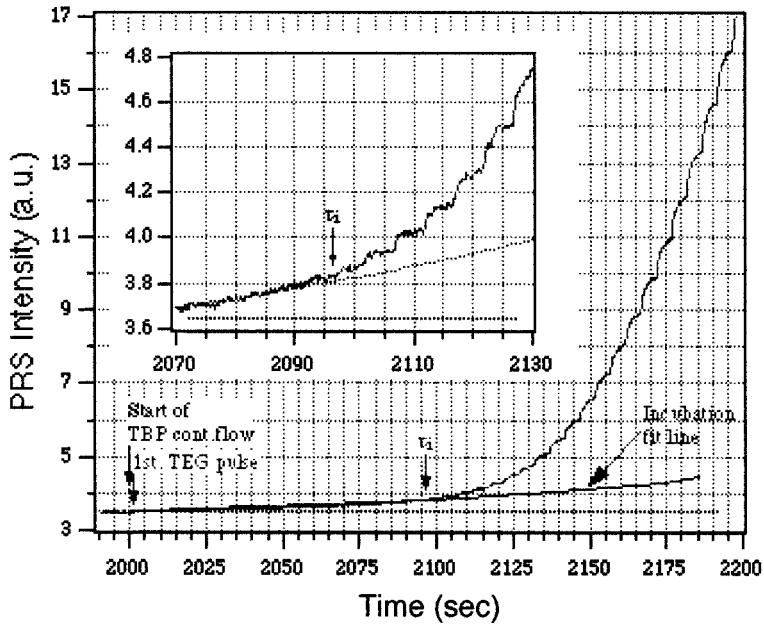
Real time monitoring of growth was accomplished by PRS, an optical probe technique that is highly sensitive to surface chemistry and is discussed in detail elsewhere (Dietz and Bachmann 1995, 1996, Dietz *et al.* 1995, Bachmann *et al.* 1998). Structural analysis of epitaxial islands was performed in cross-section and plan-view using TEM. High resolution transmission electron microscopy (HRTEM) was carried out on a JEM-4000EX microscope operating at 400 kV and that has a point to point resolution of 0.17 nm. Conventional TEM analysis was performed on a Philips EM-420 microscope operating at 120 kV and a TOPCON 002B microscope operating at 200 kV. Island distribution and morphology was examined by AFM.

### § 3. RESULTS

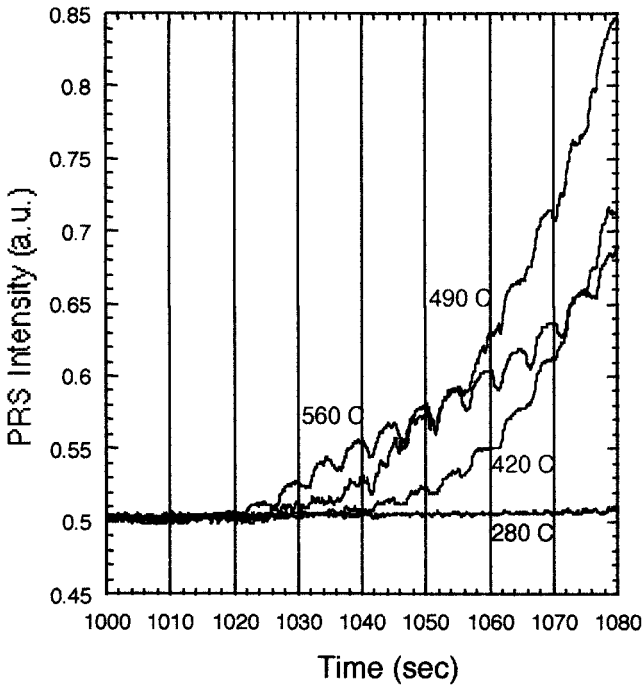
Figure 1 (*a*) depicts the PRS signal change as a function of deposition time for the epitaxial growth of GaP on (001) Si at the growth temperature of 350°C. The figure shows a monotonic increase in the PRS signal at the initial stages of growth until a critical time is reached when periodic modulation of the signal commences. This period is referred to as an incubation time ( $\tau_i$ ). Figure 1 (*b*) shows the PRS signal variation during the nucleation of GaP on (001) Si at different growth temperatures. It is evident from this figure that the incubation time decreases with increase in growth temperature.

Figure 2 (*a*) is a weak-beam, plan-view image which depicts island morphology after 80 s of growth at 420°C. Figure 2 (*b*) is an AFM scan of the same sample in which a lighter contrast corresponds to a higher elevation. The TEM image indicates a high density of islands ( $3.4 \times 10^{14} \text{ m}^{-2}$ ) that are essentially isotropic in shape and are evenly distributed with an average size of 20–25 nm. The AFM image indicates similar shapes for the islands seen in the TEM image, however the average sizes of the islands are between 35–40 nm. The AFM image also clearly shows evidence of smaller islands interspersed between the larger islands. Figure 2 (*c*) is a dark-field, plan-view image which depicts island morphology after 80 s of growth at 560°C. The image exhibits islands that are elongated along the  $\langle 110 \rangle$  directions. In particular, two islands that are elongated in two mutually perpendicular directions (indicated by the two black arrows) are seen contiguous to each other. These islands also have 'deposits' on one of the smaller facets. The island size varies between 75–100 nm in length and 25–30 nm in width. The island density is, however, an order of magnitude lower ( $1.45 \times 10^{13} \text{ m}^{-2}$ ). Figure 2 (*d*) is an AFM scan of the same sample. This image corroborates the previous TEM image, with similar island density ( $1.9 \times 10^{13} \text{ m}^{-2}$ ) and island size which varies between 80–120 nm in length and 30–35 nm in width, but in addition shows the presence of much smaller islands in the vicinity of the larger ones.

Figure 3 is a cross-sectional view along a  $\langle 110 \rangle$  direction of the islands shown in figure 2. Figures 3 (*a*) and (*b*) correspond to islands grown at 420°C. Their average height and width are 8 nm and 18 nm, respectively and are faceted on  $\{111\}$  and near



(a)



(b)

Figure 1. (a) PRS signal change as a function of deposition time for epitaxial growth of GaP islands on (001) Si at 350°C and (b) PRS signal variation during the nucleation of GaP islands on (001) Si at different growth temperatures.

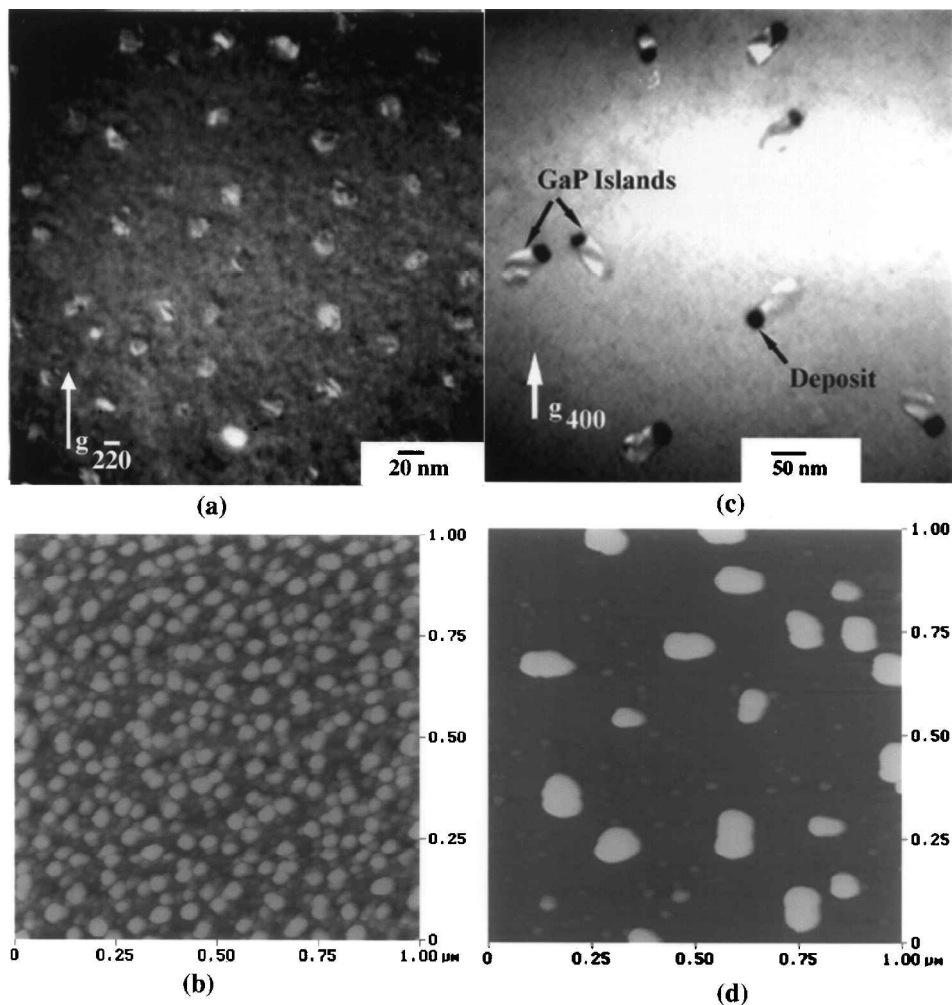


Figure 2. (a) Weak-beam plan-view image which depicts GaP island morphology after 80 s of growth at 420°C on (001) Si, (b) AFM scan of the same sample described in (a), (c) dark-field plan view image which depicts GaP island morphology after 80 s of growth at 560°C on (001) Si and (d) AFM scan of the sample described in (c). Note the differences in island shape, size and number density at the two growth temperatures.

{110} ( $6^\circ$  off) planes. Both the islands exhibit twins parallel to the {111} planes. Figure 3(c) shows an island grown for 80 s at 560°C that is faceted on {113} and {112} planes and free of planar defects. This island is 15 nm in height and more than 30 nm in width. Figure 3(d) shows deposits on a {111} facet of an island grown on at 560°C. An interesting observation is that the zincblende structure transforms near the edge of the {111} facet to the wurtzite structure. In addition, the wurtzite stacking is evident albeit faintly even within the deposit.

Figure 4(a) is a dark-field, plan-view image of GaP islands grown on (111) Si after 300 s of growth at 560°C. The image reveals two types of islands that are very sharply faceted. The first kind has six sides with the opposite sides parallel and

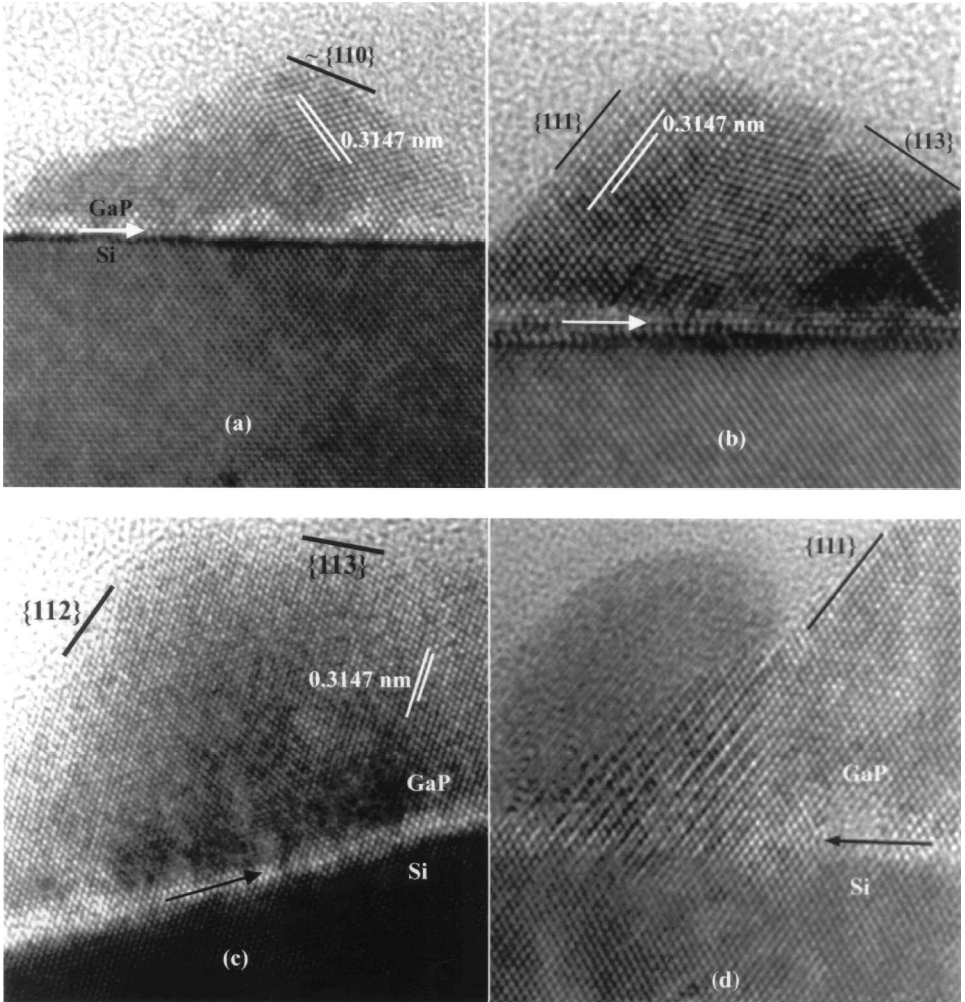


Figure 3. (a), (b) HRTEM cross-sectional images in a  $\langle 110 \rangle$  zone that show GaP islands after 80 s of growth at  $420^\circ\text{C}$  on (001) Si, (c) HRTEM image of a GaP island after 80 s of growth at  $560^\circ\text{C}$  on (001) Si and (d) HRTEM image of a deposit on the  $\{111\}$  facet of a GaP island after 80 s of growth at  $560^\circ\text{C}$  on (001) Si. Note the presence of  $\{111\}$ ,  $\{113\}$   $\{110\}$  and  $\{112\}$  facets in islands at the two growth temperatures.

unequal. The second type of island is elongated with opposite sides near parallel and equal in size. Figure 4(b) is an example of an island of the first type where the island sides are oriented close to the three  $\langle 110 \rangle$  type directions lying within the (111) surface. Figure 4(c) shows an island of the second type. Here one of the parallel sides is much longer than the other two leading to the anisotropy in island shape. The islands show a large variation in size but the largest island is about 90 nm from tip to tip. The island number density including both types of islands is close to  $10^{13} \text{ m}^{-2}$ . Figure 4(d) is an AFM image of the same sample that indicates the presence of smaller islands adjacent to the larger ones. Island size analysis from the AFM image indicated that there were a few islands that are higher than 40 nm but on average the island heights were in the range of 15–20 nm.

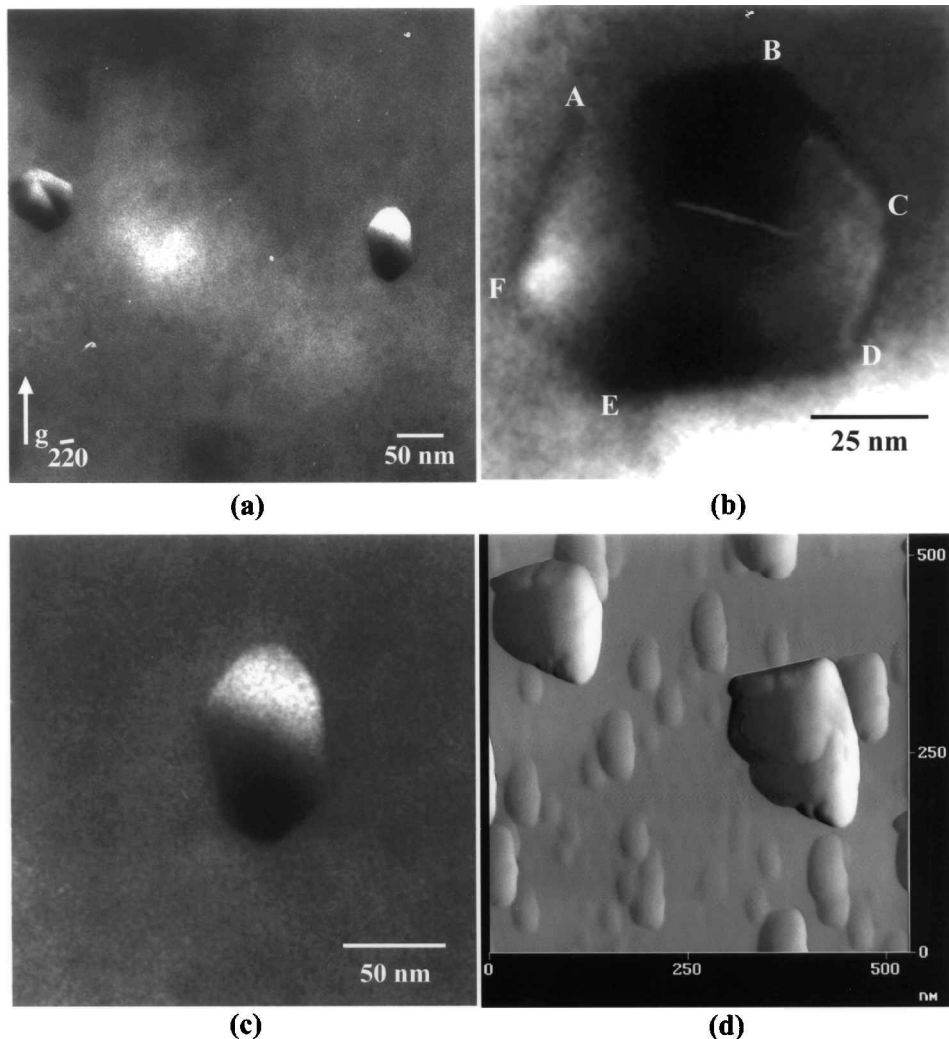


Figure 4. (a) Dark-field plan-view image which shows two different island types after 300 s of growth at 560°C on (111) Si. (b), (c) are enlarged images of the the two different island morphologies. (d) AFM scan of the sample described in (a).

In figure 5, the ‘hut’ shaped island exhibits a wurtzite GaP phase sandwiched between two zincblende GaP domains. This island has near vertical facets and  $\{110\}$  and  $\{112\}$  type sloping facets. In figure 6 the island shows only the zincblende structure and has very small vertical facets with the shallow facets dominating. This island has a similar shape as the cap on the ‘hut’ shaped island.

Figure 7 shows the growth of GaP on Si (110) and Si (113) after 100 s of growth at 420°C. The epitaxial layers on both surfaces are continuous at such an early stage of growth, and the rough morphology indicates that the layers nucleated as flat near two-dimensional (2D) islands which may have coalesced at an early stage to form a continuous film. The (110) films are slightly thicker with an average height of about 10 nm and the (113) films have a thickness of about 8 nm. In addition, the GaP–Si interface is continuous and smooth in both films.

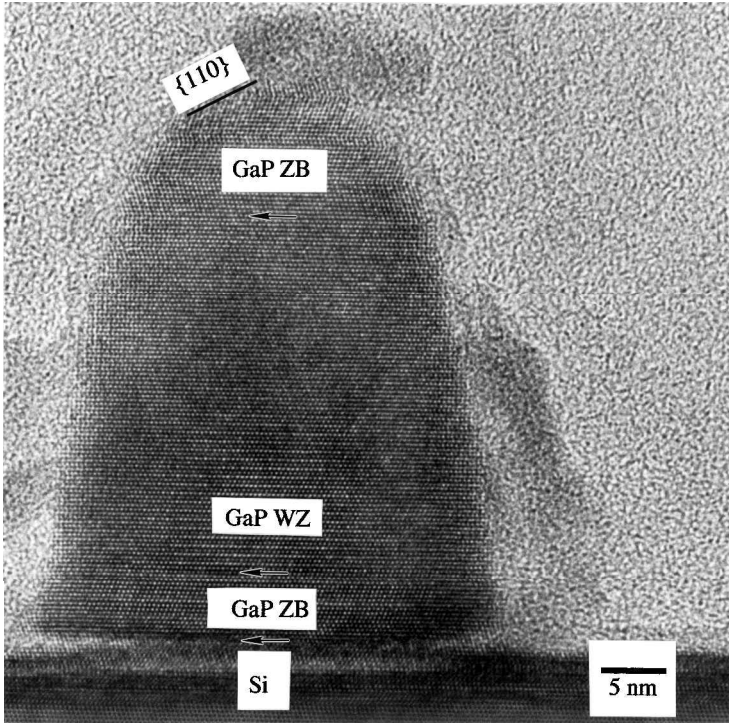


Figure 5. HRTEM cross-sectional image in a  $\langle 110 \rangle$  zone of a GaP island on (111) Si after 300 s of growth at 560°C. Note the coexistence of the zincblende (GaP ZB) and wurtzite (GaP WZ) domains within the same island.

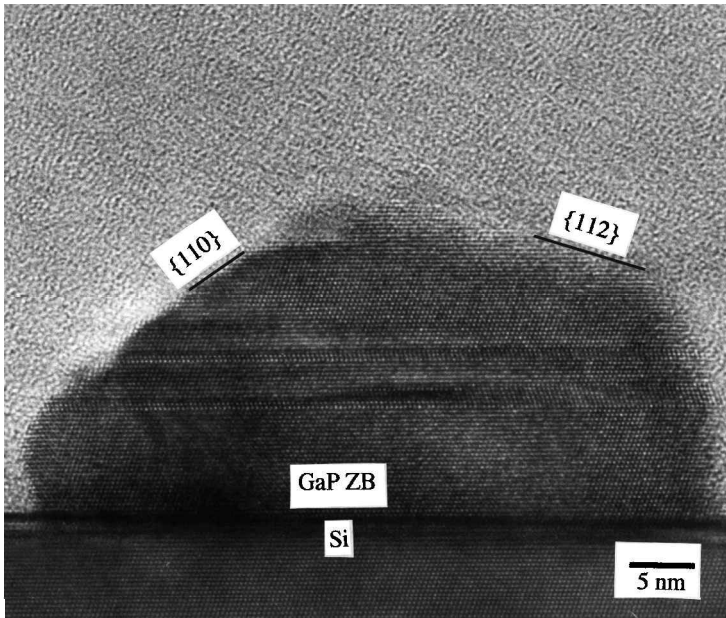


Figure 6. HRTEM cross-sectional image in a  $\langle 110 \rangle$  zone of a GaP island on (111) Si after 300 s of growth at 560°C. Note the absence of the wurtzite polytype in this island.

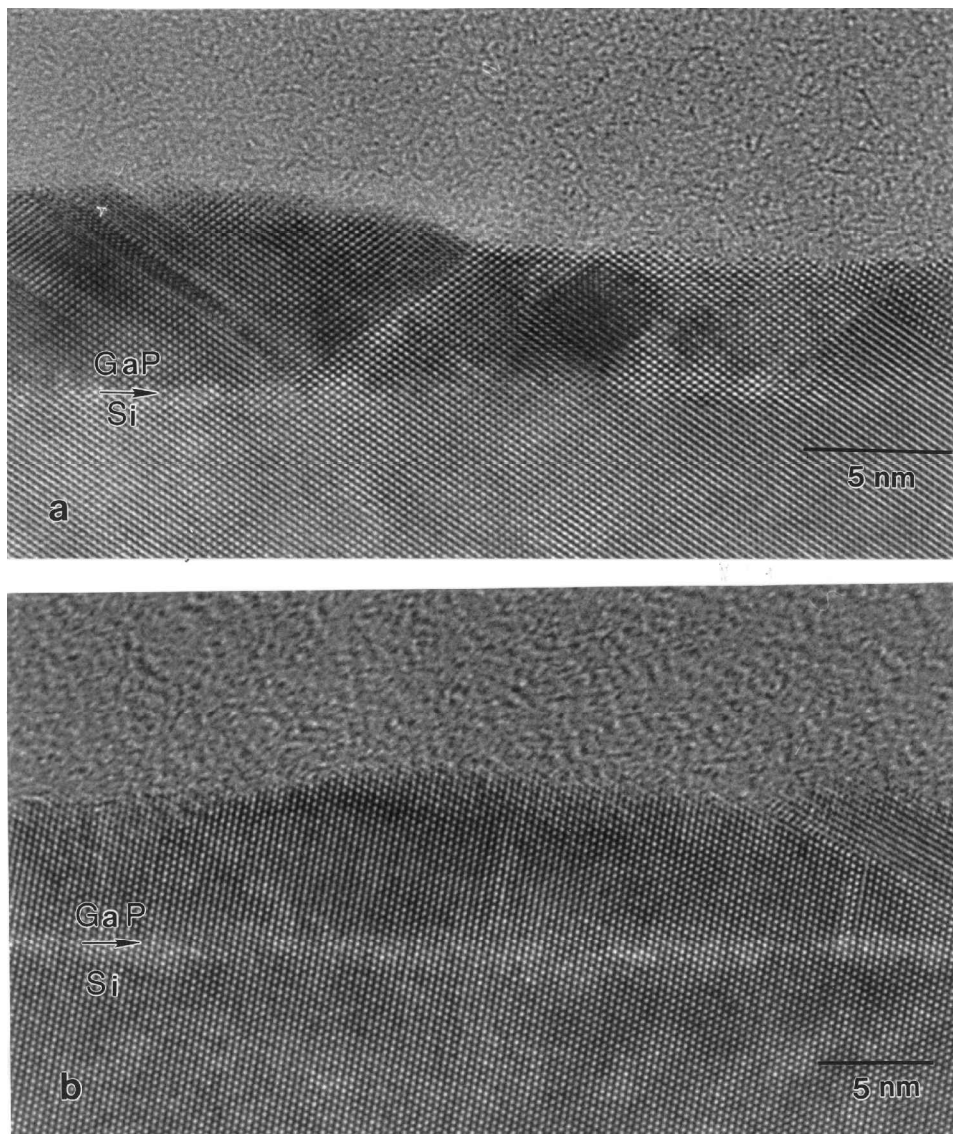


Figure 7. HRTEM cross-sectional images in a  $\langle 110 \rangle$  zone of GaP epitaxial layers after 100 s of growth at 420°C on (a) (110) Si and (b) (113) Si.

#### §4. DISCUSSION

Important observations emerging from the preceding results are the following. First, the epitaxial layer nucleates as faceted three-dimensional (3D) islands on (001) and (111) Si. There exists a characteristic incubation time for island nucleation that varies as a function of temperature. Second, island morphology and nucleation density vary with temperature for islands grown on (001) Si. At lower temperatures, the islands are smaller in size, have a higher number density and are isotropic in shape. In contrast, at higher temperatures and for the same growth time, the islands are larger in size, have a lower number density and are elongated along the  $\langle 110 \rangle$  directions in (001) Si. Third, islands grown on (111) Si have a truncated hexagonal

shape with unequal parallel sides oriented along the three  $\langle 110 \rangle$  directions in (111) Si. In addition wurtzite GaP has been observed to coexist with the zincblende polytype in some of the islands. Fourth, nearly flat 2D islands are nucleated on (110) and (113) Si which coalesce at an early stage to form a continuous film.

The PRS signals in figures 1(a) and (b) are the reflected intensity at the initial stages of heteroepitaxy from the four layer stack of Si–GaP–surface layer–ambient. The reflectance at each of these interfaces is characterized by the dielectric constants of the media that make up the interface. The signal oscillates due to interference in the film from partial waves reflected at the ambient–GaP interface and GaP–Si interface (Bachmann *et al.* 1995a, Dietz and Bachmann 1995, 1996, Dietz *et al.* 1995). Each peak in the fine structure of the signal corresponds to a complete precursor cycle.

The origins of an incubation time are related to the process of heterogeneous nucleation of a crystal from the vapour onto a substrate. There is a critical radius associated with a growing nucleus at each temperature below which they are unstable. Increasing the temperature for a given supersaturation has the effect of increasing the size of the critical nucleus and reducing the nucleation rate. The incubation time in figure 1(a) is thus the time required to form critical size and stable nuclei on the surface of the substrate. The initial monotonic increase can be explained as a build up of a surface reaction layer consisting of the products of TEG and TBP decomposition reactions on the Si surface before the formation of stable nuclei at  $t = \tau_i$  (Sukidi *et al.* 1999). The sharp increase in the PRS signal at  $\tau > \tau_i$  is attributed to the smaller dielectric constant of a corrugated GaP film which covers the Si substrate incompletely (indicative of 3D GaP islands) when compared to the dielectric function for a continuous film (Bachmann *et al.* 1995a). The larger difference between the dielectric constants of the Si substrate and the corrugated film would express itself in an enhanced PRS intensity during the nucleation period as seen in figures 1(a) and (b). In addition, the decomposition of TBP is enhanced on GaP surfaces as compared to Si (Li *et al.* 1989, Kelliher *et al.* 1993). As a result, appearance of GaP epitaxial nuclei on Si surface and subsequent increase in GaP surface area with each increment in growth explains the step-wise increase in the PRS signal at  $\tau > \tau_i$  (Sukidi *et al.* 1999).

The observed decrease in  $\tau_i$  as seen in figure 1(b) with increasing temperature for (001) Si is unexpected since increasing size of the critical nucleus requires a higher supersaturation of the surface with precursors of growth, i.e. a longer incubation time is expected at higher temperatures. We believe this to be an effect of the increased rate of surface decomposition of source vapour molecules leading to faster evolution of critical supersaturation at higher temperatures, thus facilitating earlier nucleation.

In the previous discussion we have not considered the influence of the substrate on the nucleation of islands. During epitaxial growth, the substrate acts as a growth template and plays a critical role in the initial stages of nucleation and growth. The type of growth mode that is chosen is based on the interface energy. The interface energy is made up of two components: chemical and structural (Mahajan 1996). The chemical component depends on the type of atoms which form the interface, and the structural component depends on the lattice mismatch between epilayer and substrate. When a polar semiconductor like GaP is grown on a non-polar semiconductor like Si, the interface energy will have contributions primarily from the chemical component due to the very low lattice mismatch. On the (001) or (111) orientation of

Si, all the surface atoms are structurally alike. This removes any kind of site selectivity for the incoming adatoms during growth. In addition, it is known that P has a stronger tendency to bond with Si, thus leading to the first monolayer being mostly P. The presence of an extra electron per surface atom (on average) in the first layer would lead to the build up of an interface charge at the polar GaP–Si (001) and GaP–Si (111) heterojunctions (Harrison *et al.* 1978). Such an interface charge would increase the energy of the heterointerface. As a result, incoming adatoms would prefer to bond to already nucleated GaP islands where the GaP–GaP homointerface does not suffer from the problem of interface charge. This facilitates island growth as confirmed by our TEM and AFM results.

Variations in size and number density of islands at different temperatures for (001) Si from figure 2 are consistent with the aforementioned theory of nucleation and growth. For a given supersaturation, low temperatures correspond to higher nucleation rates and this ensures a higher island number density in comparison to those observed at higher temperatures. Further, a lower incubation time and higher atomic mobility at higher temperatures predict that islands once formed maintain a higher growth rate at the initial stages after nucleation. This leads to larger size of islands for the same growth period at higher temperatures. The presence of smaller islands in the AFM images of figure 2 can be understood in terms of a characteristic capture radius associated with each stable nucleus. If the incoming adatoms do not fall within this radius, the atoms would prefer to form new nuclei. When the distance between stable nuclei is less than the capture radius, incoming adatoms would prefer to attach themselves to the stable nuclei and this results in a rapid decrease in the nucleation rate and growth prevails. The difference in size of islands in the TEM and AFM images is attributed to a much larger sampling space in the AFM scans as compared to a localized area for the TEM image, therefore AFM images would be more representative of actual size. However, when the islands are closely spaced together the AFM tip may encounter a new island before touching the substrate and therefore this makes it difficult to actually discern true island size. The absence of small islands in the TEM images especially figure 2(c) is again attributed to a smaller imaging area and in addition, chemical thinning for plan-view images leads to large differences in sample thickness, which make it very difficult to discern small features in the image. In this regard, AFM is more sensitive since it can map out features as a function of height.

Figure 3 shows that the islands are faceted on the  $\{111\}$ ,  $\{113\}$ ,  $\{110\}$  and  $\{112\}$  planes. They exhibit marked shape anisotropy at 560°C which is absent at 420°C. The tendency to form facets in crystalline nuclei is due to the variation in surface energy with crystallographic orientation. As a consequence, epitaxial nuclei are faceted parallel to low energy crystallographic planes to reduce their surface energy. In both diamond and zincblende structures, the lowest energy planes are the close packed  $\{111\}$  planes. Thus, GaP nuclei formed on (001) Si would be bounded by the four  $\{111\}$  planes. However, all four  $\{111\}$  type facets are not equivalent because two are terminated by Ga and two by P due to the non-centrosymmetry of the zincblende structure. Hence, assuming that epitaxial nuclei possess only  $\{111\}$  type facets (an idealization of the actual situation), the nucleus could take the shape of a truncated prism as shown in figure 8(a). To minimize the total energy, facets with a higher surface energy will have a lower surface area. If we consider only the electronic component, the surface energy to a first approximation is directly proportional to the dangling bond density. Each P atom has a lone pair of electrons

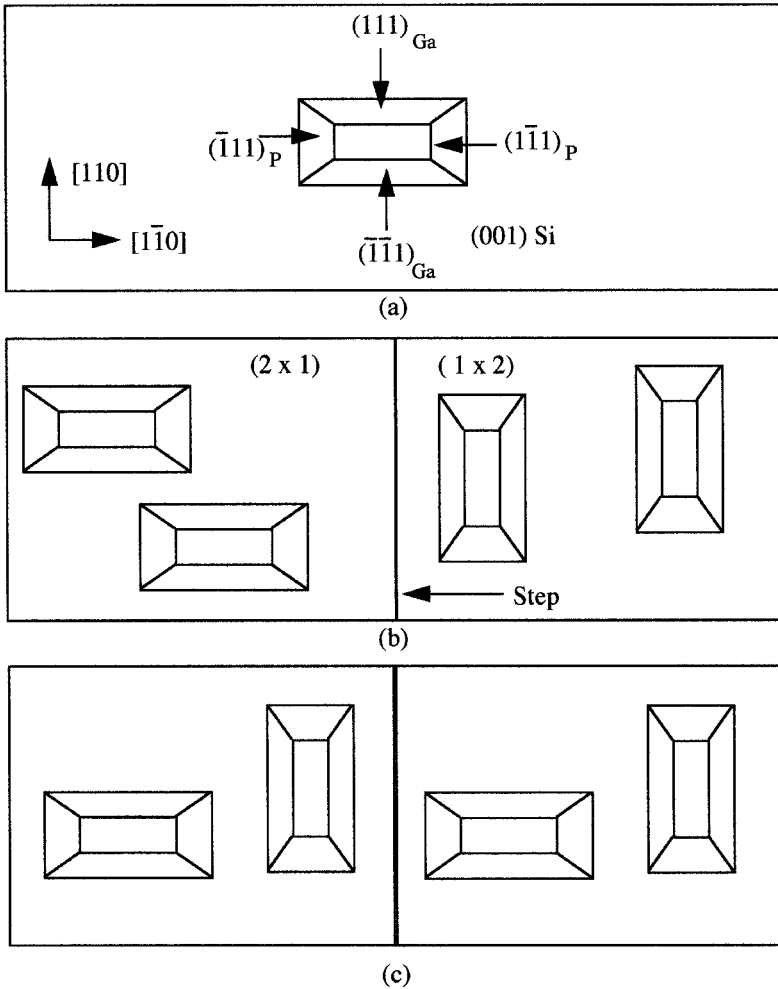


Figure 8. (a) Possible shape of a GaP island nucleated on (001) Si that is faceted on  $\{111\}$  planes, (b) GaP islands nucleated on  $(2 \times 1)$  and  $(1 \times 2)$  reconstructed terraces that are separated by a  $[110]$ -type monatomic step on (001) Si and (c) GaP islands randomly nucleated on unreconstructed terraces that are separated by a  $[110]$ -type monatomic step on (001) Si.

when it terminates the surface and contributes to two dangling bonds. On the other hand, Ga has no dangling bonds when it terminates the surface. Thus, the  $\{111\}_{\text{P}}$  surfaces should have a higher surface energy and hence a smaller surface area. However, temperature plays a crucial role in the development of these facets. At lower temperatures, inadequate thermal energy reduces atomic mobility and atoms tend to stick wherever they land. Restricted kinetics thus prevent adatoms from arranging themselves in low energy configurations and the island shape is irregular and undefined and gives the impression of being rounded. At higher temperatures enhanced atomic mobility relaxes the kinetic limitation and stable facets can be generated. Growth at these temperatures would then occur at the expense of the facet with a higher surface energy and therefore a high degree of anisotropy in facet shape is expected. This explains the observed effect of temperature on island shape.

Another interesting observation from figure 2 (c) is that islands are elongated in the mutually perpendicular  $\langle 110 \rangle$  directions with approximately the same propensity. Aspnes and Ihm (1987) and Kroemer (1987a, b) have suggested that on Si (001) exactly oriented reconstructed surfaces the most common step height is one atomic layer. Further, two distinct monatomic steps are observed which differ only with respect to the orientation of the surface dangling bonds in reference to the step edge. The terraces separated by these steps are terminated by Si atoms of a different sublattice and can show  $(2 \times 1)$  and  $(1 \times 2)$  reconstructions, respectively. In as much as P forms strong bonds with Si, whereas Ga does not, the first atomic layer bonding to the Si might be expected to be a P layer. If the growth is governed by surface reconstruction, a uniform distribution of islands all elongated along a  $\langle 110 \rangle$  direction would be separated from a uniform distribution of islands elongated in the perpendicular  $\langle 110 \rangle$  direction by a monatomic step (figure 8 (b)). Our results from figure 2 (b) would imply a very non-uniform distribution of  $\langle 110 \rangle$  steps. We believe, therefore, that surface reconstruction may not have a role in the nucleation of GaP islands on (001) Si. Since in Si the two  $\langle 110 \rangle$  directions in the (001) surface are crystallographically identical, the probability of elongation in these two directions is equal. Thus, the islands oriented along the  $[110]$  and  $[\bar{1}\bar{1}0]$  directions can be nucleated on the same terrace, as depicted in figure 8 (c).

The presence of  $\{113\}$  facets in figures 3 (b) and (c) (right facets) implies that this high index surface is stable at both of these temperatures. The ideal  $\{113\}$  surface is unique in that it contains an equal number of step and terrace atoms (Chadi 1984). In fact, there are two atoms per unit cell which are two-fold and three-fold coordinated. In a III-V material like GaP, there are two  $\{113\}$  charge neutral surfaces which differ only in an interchange of Ga and P atoms on the two sites (see figure 10 (d) later), exchange the two Si surface atoms with Ga and P atoms). These facets have been known to occur in epitaxial GaAs islands (Vila *et al.* 1997), wherein the stability of the  $\{113\}$  surface is attributed to the electrical neutrality of such a surface due to an equal number of Ga and As atoms. The presence of these facets in the GaP islands provides further experimental evidence that these facets are indeed stable in III-V islands despite their higher surface energy. (Assuming the surface energy to be proportional to the density of broken bonds ( $n$ ),  $n_{113} = (12/11^{1/2})a^2$  and  $n_{111} = (4/3^{1/2})a^2$ , where  $a$  is the lattice constant.)

The presence of deposits at 560°C has been observed in both plan-view (figure 2 (b), shorter facets) and cross-sectional (figure 3 (d),  $\{111\}$  facets) micrographs. Elemental maps using electron energy loss spectroscopy and line scans using energy dispersive X-ray analysis were not conclusive on the elemental composition of the deposit, although a large variation in signal did not occur as we moved from the island to the deposit. The observation that contiguous to the deposit the stacking sequence of the  $\{111\}$  facet changes from a zincblende to the wurtzite  $\{0001\}$  implies that there are kinetic constraints to growth on this facet which allow the transformation. The faint outline of the wurtzite structure in the deposit combined with the observation that these deposits are noticed only on shorter  $\{111\}$  facets of these islands imply different growth conditions on this facet. If indeed the shorter facet is a P-terminated  $\{111\}$  facet then the presence of the deposit could be attributed to a lowered surface mobility for incoming atoms due to the higher dangling bond density of a P-terminated  $\{111\}$  facet as compared to a  $\{111\}$  Ga-terminated facet. Thus incoming adatoms are immobilized as they land and may not reach their equilibrium positions.

TEM and AFM results have shown discrete islands being present on the (111) Si surface even after 300 s of growth. Previous PRS results (Sukidi *et al.* 1999) have revealed that the incubation time is strongly dependent on substrate orientation with  $\tau_i(001) < \tau_i(111)$  at 560°C. The reasons for such a dependence are as yet unclear, but may be a consequence of a lowered density of dangling bonds on the (111) surface ( $1/3^{1/2}$  that on the (001) surface).

Plan-view images (figure 4) of these islands has revealed that they are hexagonal in shape with the parallel sides oriented close to the three  $\langle 110 \rangle$  directions in (111) Si. In addition, both plan and cross-sectional views have brought to light two different island morphologies under the same growth conditions. For both these island types, we believe that the initial growth proceeds parallel to the  $\{111\}$  facets inclined to the interface. This implies that in plan view the sides of the hexagon should lie parallel to the line of intersection of the inclined facets with the substrate. A schematic of the possible shape is illustrated in figure 9 (a). The presence of unequal parallel sides is

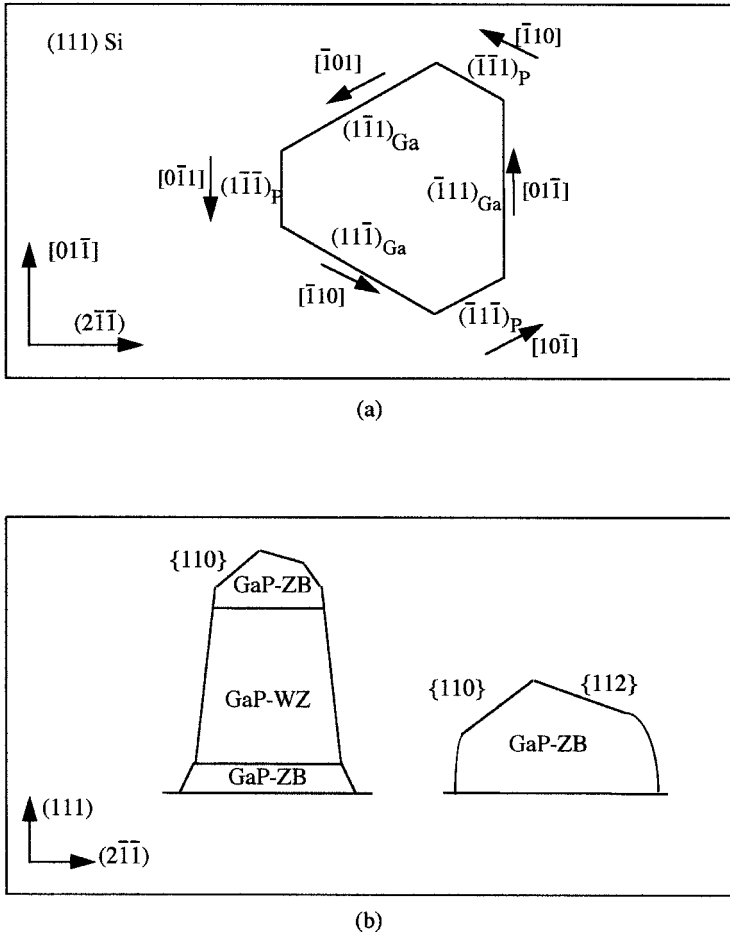


Figure 9. (a) Possible shape of a GaP island nucleated on (111) Si viewed along  $[11\bar{1}]$ ; the planes depicted within the island are  $\{111\}$  type inclined facets which have a  $\langle 110 \rangle$  trace on the (111) Si surface. (b) Cross-sectional view of the two types of GaP islands on (111) Si viewed along  $[01\bar{1}]$ .

due to the lack of inversion symmetry in the zincblende structure. Thus, opposing facets in the hexagon would be terminated by different species and therefore by the surface energy arguments developed before, facet size would also be different. It is to be noted here, however, that we have not yet been able to match the two island types in cross-sectional views to those in plan-view. We do not know, therefore, if the hut shaped island in figure 5 corresponds to the island in figure 4 (b) or (c).

The sloping facets in the shallower island in figure 6 are close to a  $\{110\}$  and  $\{112\}$  orientation (figure 9 (b)). In addition,  $\{110\}$  and  $\{112\}$  facets are seen in figure 3 (a) and figure 3 (c). The  $\{110\}$  planes in GaP, as shown in figure 10 (a),

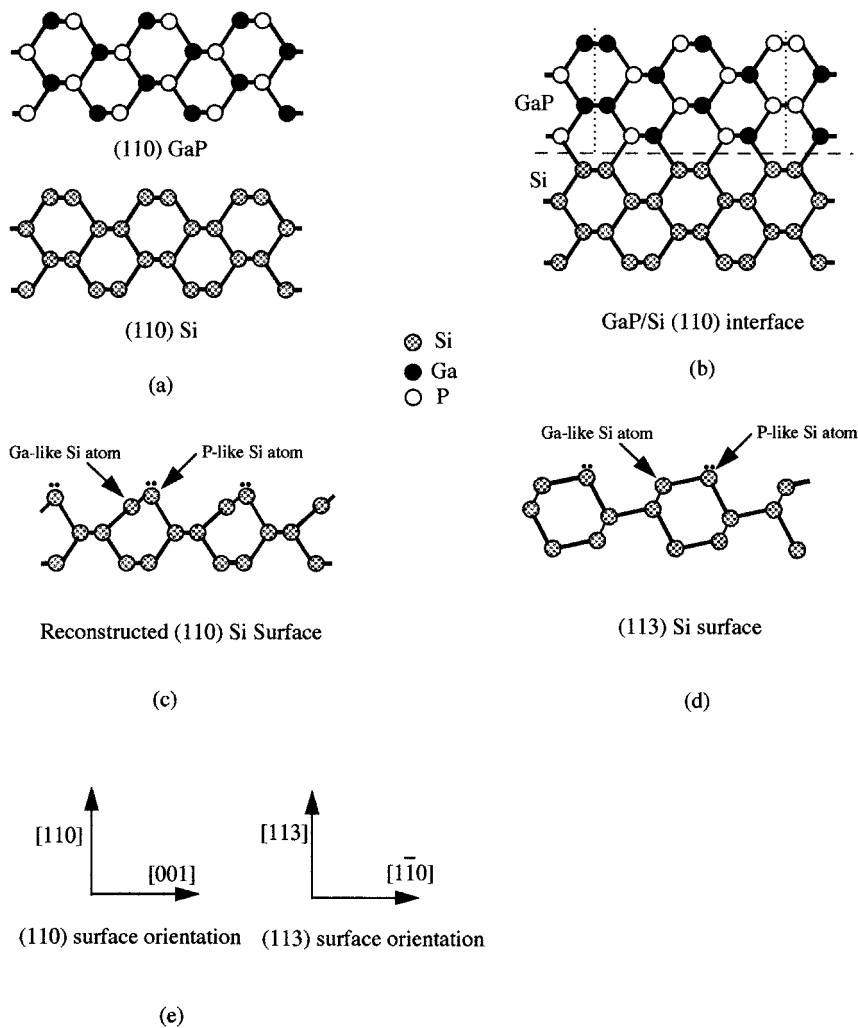


Figure 10. (a) (110) GaP and (110) Si surfaces viewed in cross-section along  $[1\bar{1}0]$ , (b) bond mismatching at the GaP-Si (110) surface in the absence of site selectivity that leads to inversion domain boundaries depicted by the dashed lines, (c) growth-induced reconstruction of the (110) Si surface which provides selective sites for the bonding of Ga and P atoms, (d) (113) Si surface viewed in cross-section to illustrate the possibility of site selectivity similar to the (110) surface and (e) identification of crystallographic directions for the two surfaces.

have an equal number of Ga and P atoms on the surface rendering each successive plane electrically neutral during growth. Thus similar to the {113} facets, the higher dangling bond density on the {110} surface as compared to that of the {111} surfaces ( $n_{110}/n_{111} = 1.224$ ) may be compensated by electrical neutrality of the non-polar surface. The {112} surface is very similar to the {110} surface in that each plane has an equal number of Ga and P atoms, but in addition like the {113} surface, the two surface atoms have a different number of dangling bonds allowing for site selectivity during growth. Thus a combination of site selectivity and charge neutrality may stabilize this facet. It is to be noted that facet type is being determined by measurement of angles subtended between facets and compared to angles between low-index planes. In addition, the shape of islands exhibits some roundness which further induces errors in such an estimate.

It is envisaged that the presence of two different types of island morphologies on (111) Si under the same growth conditions could be a consequence of variation in the concentration of active species across the wafer. The increased incubation time on the (111) surface implies that the growth environment is rich with the active species before nucleation occurs. This ensures a high growth rate after initial nucleation. Thus, when a hut shape island is nucleated (figure 5), growth proceeds initially as the zincblende polytype governed by the diamond cubic Si template and the ...A(Ga)*a*(P)B(Ga)*b*(P)C(Ga)*c*(P)A(Ga)*a*(P)... stacking for the (111) planes is maintained. However, a higher growth rate due to increased supersaturation may provide the necessary kinetic pathway to stabilize the otherwise higher energy wurtzite phase. Thus, although the equilibrium phase for GaP is zincblende, the wurtzite phase may be stabilized by kinetic considerations. Coexistence of the wurtzite and zincblende phases for GaN has been reported by Yang *et al.* (1995) although the two phases were produced by changing the growth temperature. We believe that this is the first time that the wurtzite phase of GaP has been observed. In addition, this is the first time that wurtzite and zincblende phases have been shown to coexist at the same growth temperature during epitaxial growth. In contrast to figure 5, in figure 6 a low species concentration might prevent the nucleation of the wurtzite polytype and allow low energy facets to develop at an early stage.

GaP grows on the (110) and (113) surfaces of Si have shown very similar morphologies which are very different from those obtained on the (001) and (111) surfaces. The ideal (110) unreconstructed Si surface has an unit cell of two atoms that are chemically identical and have the same back bonds to the substrate (figure 10 (a)). The only difference between the two sites is the orientation of the tetrahedral bonds in space. To maintain the symmetry of (110) GaP surface, both Ga and P atoms are needed at the Si (110) surface. This could lead to the formation of copious inversion domain boundaries where like atoms are bonded with each other as explained in figure 10 (b). These domain boundaries are bound to be very highly charged and would lead to deviations from good (110) morphology (Kroemer *et al.* 1980). Our results on (110) Si of nearly flat film morphology proves otherwise indicating that there is definitely some kind of site selectivity on the surface. Kroemer *et al.* (1980) have argued that to prevent the formation of these presumably higher energy domain configurations during growth, the Si surface reconstructs in such a manner so as to depress one of the two atoms in each surface unit cell. This reconstruction leads to a redistribution of electrons in such a way that the raised row gains an electron and the depressed row loses an electron as shown in the figure 10 (c). The atoms in the raised row thus mimic the electronic configuration of P while the

atoms in the depressed row become Ga-like. This growth-induced reconstruction would then provide the required site selectivity for growth with the reduced density of inversion domain boundaries.

The growth-induced reconstruction of the (110) surface would also mimic the surface configuration of the unreconstructed (113) surface. The surface unit cell of the (113) Si surface has two atoms which are two-fold and three-fold coordinated. The two-fold coordinated Si atoms would be P-like while the three-fold coordinated Si atoms would be Ga-like, rendering a nearly identical site selectivity to that of the previously discussed (110) surface (figure 10 (*d*)). The enhanced site selectivity on such a surface would ensure that the first layer of growth contains both Ga and P species thus rendering the interface electrically neutral due to the net interface charge being nearly zero. This would reduce the energy of the heterointerface, and the layer would wet the substrate surface more uniformly. This is supported by our HRTEM images of figure 7 which shows a flatter more uniform morphology for the GaP film grown on the (110) Si and (113) Si surfaces.

#### § 5. CONCLUSIONS

- (1) The initial stages of GaP growth on (001) Si exhibit an incubation period which is influenced by growth temperature. The observed reduction in incubation time with increase in temperature is attributed to the increased rate of surface decomposition of source vapour molecules leading to faster evolution of critical supersaturation at higher temperatures, even though the size of the critical nucleus for a given supply rate of source vapour molecules increases with increasing temperature.
- (2) The shape, size and number density of epitaxial islands grown on (001) Si are sensitive to growth temperature. Higher temperatures are characterized by increased shape anisotropy such that islands are elongated along the two mutually perpendicular  $\langle 110 \rangle$  directions in (001). This observation is explained as a combined effect of lower incubation period and enhanced atomic mobility at higher temperatures which allows the formation of stable facets.
- (3) Wurtzite GaP has been shown to coexist with zincblende GaP domains for a few islands grown on (111) Si at 560°C. This is attributed to a high species supersaturation which kinetically stabilizes the wurtzite phase.
- (4) The growth-induced reconstructed (110) surface and (113) Si surface could provide specific surface sites for the bonding of Ga and P atoms within the same layer, thereby preventing inversion domains and facilitating a nearly charge neutral interface. This concept is used to explain the excellent film morphology on both these surfaces. The presence of flat near 2D islands is an indication that (110) and (113) Si surfaces may provide a better template for growth and prevent problems associated with growth and subsequent coalescence of faceted 3D islands on (001) and (111) Si.

#### ACKNOWLEDGEMENTS

The authors gratefully acknowledge the support of this work by DOD-MURI grant F49620- 95-1-0447.

## REFERENCES

- ASPNES, D. E., and IHM, J., 1987, *Heteroepitaxy on Silicon II, Materials Research Society Symposium Proceedings*, Vol. 91, edited by J. C. C. Fan, J. M. Phillips and B. Y. Tsaur (Pittsburgh, Pennsylvania: Materials Research Society), pp. 45–50.
- BACHMANN, K. J., DIETZ, N., MILLER, A. E., VENABLES, D., and KELLIHER, J. T., 1995a, *J. Vac. Sci. Technol. A*, **13**, 696.
- BACHMANN, K. J., ROSSOW, U., and DIETZ, N., 1995b, *Mater. Sci. Eng. B*, **35**, 472.
- BACHMANN, K. J., SUKIDI, N., HOPFNER, C., HARRIS, C., DIETZ, N., TRAN, H. T., BEELER, S., ITO, K., and BANKS, H. T., 1998, *J. Cryst. Growth*, **183**, 323.
- CHADI, D. J., 1984, *Phys. Rev. B*, **29**, 785.
- DIETZ, N., and BACHMANN, K. J., 1995, *MRS Bull.*, **20**, 49; 1996, *Vacuum*, **47**, 133.
- DIETZ, N., MILLER, A., KELLIHER, J. T., VENABLES, D., and BACHMANN, K. J., 1995, *J. Cryst. Growth*, **150**, 691.
- ERNST, F., and PIROUZ, P., 1988, *J. appl. Phys.*, **64**, 4526; 1989, *J. mater. Res.*, **4**, 834.
- GERTHSEN, D., BIGELSEN, D. K., PONCE, F. A., and TRAMONTANA, J. C., 1990, *J. Cryst. Growth*, **106**, 157.
- HADLEY, M. J., TEAR, S. P., ROTTGER, B., and NEDDERMEYER, H., 1993, *Surf. Sci.*, **280**, 258.
- HARRISON, W. A., KRAUT, E. A., WALDROP, J. R., and GRANT, R. W., 1978, *Phys. Rev. B*, **18**, 4402.
- KELLIHER, J. T., THORNTON, J., DIETZ, N., LUCOVSKY, G., and BACHMANN, K. J., 1993, *Mater. Sci. Eng. B*, **22**, 97.
- KNALL, J., and PETHICA, J. B., 1992, *Surf. Sci.*, **265**, 156.
- KROEMER, H., 1987a, *J. Cryst. Growth*, **81**, 193; 1987b, *J. Vac. Sci. Technol. B*, **5**, 1150.
- KROEMER, H., POLASKO, K. J., and WRIGHT, S. C., 1980, *Appl. Phys. Lett.*, **36**, 763.
- LI, S. H., LARSEN, C. A., BUCHAN, N. I., and STRINGFELLOW, G. B., 1989, *J. appl. Phys.*, **65**, 5161.
- MAHAJAN, S., 1996, *Covalent Ceramics III: Science and Technology of Non-oxides, Materials Research Society Symposium Proceedings*, Vol. 410, edited by A. F. Hepp, P. N. Kumta, J. J. Sullivan, G. S. Fischman and A. E. Kaloyeros (Pittsburgh, Pennsylvania: Materials Research Society), pp. 3–15.
- SOGA, T., GEORGE, T., SUZUKI, T., UMEMO, M., and WEBER, E. R., 1991, *Appl. Phys. Lett.*, **58**, 2108.
- SOGA, T., JIMBO, T., and UMEMO, M., 1994, *Appl. Surf. Sci.*, **82–83**, 64; 1996, *J. Cryst. Growth*, **163**, 165.
- SUKIDI, N., BACHMANN, K. J., NARAYANAN, V., and MAHAJAN, S., 1999, *J. Electrochem. Soc.*, **146**, 1147.
- VILA, A., CORNET, A., and MORANTE, J. R., 1997, *Mater. Lett.*, **31**, 339.
- VILA, A., CORNET, A., MORANTE, J. R., and RUTERANA, P., 1993, *Microscopy of Semiconducting Materials 1993*, edited by A. G. Cullis, A. E. Staton-Bevan and J. L. Hutchison (Bristol, England: Royal Microscopical Society), pp. 353–356.
- YANG, J. W., KUZNIA, J. N., CHEN, Q. C., KHAN, M. A., GEORGE, T., DE GRAEF, M., and MAHAJAN, S., 1995, *Appl. Phys. Lett.*, **67**, 3759.
- YODO, T., TAMURA, M., LOPEZ, M., and KAJIKAWA, Y., 1994, *J. appl. Phys.*, **76**, 7630.